Hybrid Wireless-Wired Optical Sensor for Extreme Temperature Measurement in Next Generation Energy Efficient Gas Turbines

Nabeel A. Riza
Mumtaz Sheikh
Frank Perez[1]

Photonic Information Processing Systems Laboratory,
CREOL, The College of Optics and Photonics,
University of Central Florida,
4000 Central Florida Boulevard,
Orlando, FL 32816

Accuracy, reliability, and long lifetimes are critical parameters for sensors measuring temperature in gas turbines of clean coal-fired power plants. Greener high efficiency next generation power plants need gas turbines operating at extremely high temperatures of 1500°C, where present thermocouple temperature probe technology fails to operate with reliable and accurate readings over long lifetimes. To solve this pressing problem, we have proposed the concept of a new hybrid class of all-silicon carbide (SiC) optical sensor, where a single crystal SiC optical chip is embedded in a sintered SiC tube assembly, forming a coefficient of thermal expansion (CTE) matched all-SiC front-end probe. Because chip and host material are CTE matched, optimal handling of extreme thermal ramps and temperatures is possible. In this article, we demonstrate the first successful industrial combustor rig test of this hybrid all-SiC temperature sensor front-end probe indicating demonstrated probe structural robustness to 1600°C and rig test data to ~1200°C. The design of the rig test sensor system is presented and data are analyzed. [DOI: 10.1115/1.3204509]

Keywords: temperature sensor, extreme environments, gas turbines, optical sensor

1 Introduction

Coal continues to be the dominant fossil fuel around the world used for electric power production. The increasing thirst for energy consumption, particularly in developing economies such as China and India, is leading to rapid deployment of large (>300 MW) coal-fired power plants. Per 2008 data, China was building two or more power plants a month. Given the negative environmental effects of coal technology, the research community and power plant technology manufacturers are developing methods for greener energy production via cleaner coal-based fuels [1–4]. Even the jet engine industry is pushing for super-hot turbines to enable faster, longer range, and more fuel efficient planes [5]. In addition, maritime transportation can also benefit from more efficient on-board power and propulsion systems [6,7]. Specifically, the next generation power plants are being designed using cleaner natural gas produced by coal gasification systems. Compared with older combustion systems operating near the 1000°C temperature with on average 32% efficiencies, the new combined-cycle power plants are being designed for operations at much higher 1500°C temperatures. Recent studies are showing that operating the gas turbines at these elevated temperatures will not only produce energy with higher on average 60% efficiencies of scale per laws of thermodynamics, but operating the combustor at higher temperature can produce greener plant designs with improved methods for waste product removal and storage [8]. Given the rationale that clean coal power production will be the reality for many years to come, innovators are being pushed to develop a reliable, accurate, and long lasting (>10,000 h) temperature measurement technology to operate in the hostile environment of combustion chambers of gas turbines. Today, in test engines, the dominant temperature measurement technology is the classic thermocouple (TC) probe. Although precious metal platinum–rhodium TC probes can handle the extreme temperature measurement range, these probes require special packaging to increase operational accuracy and lifetimes. A common problem that inherently plagues TC technology in these extreme environments is that the insulating ceramic in which the TC wires are embedded develops tiny cracks that eventually lead to insulation breakdown. Specifically, the large thermal ramps and mechanical stresses the TC probe suffers cause the multimaterial probe to suffer mechanical failure due to CTE mismatch of probe materials [9]. In addition, TCs via the electromotive force (EMF) voltage-based effect have an inherent repeatability/accuracy tolerance that is a certain percentage of the temperature measured, essentially linked to the intrinsic unavoidable differences in the thermoelectric properties along the length of the wires due to the intrinsic variations in the wire alloy compositions and their annealing state [10].

Researchers have attempted designing various optical methods [11,12], specifically sapphire crystal and sapphire-fiber-based fiber-optic temperature sensors for these extreme environment applications [13–16]. Fundamentally, this approach requires the special packaging of the mechanically fragile optical fiber wire and fiber tip sensing element, again forming a multimaterial CTE mismatched assembly that is fundamentally prone to mechanical failure over plant service-time durations. Optical pyrometry [17–19] is also an attractive option for measuring extreme temperatures, in particular, when the black-body radiation emissitivity factor is constant or calibratable, such as for clean metal surfaces. As the gas mixtures in advanced gas turbines is a dynamic soup of gases, corrosive liquids, solid waste, and specific plant conditions, development is required of better emissivity models over engine lifetime operational conditions for reliable readings via active calibration. Pyrometers also face the multimaterial probe packaging limitations as radiation capture lens and/or fiber-optics has to be protected from the harsh environment of gas turbines. SiC is an excellent material for handling extreme conditions, hence previous attempts using SiC thin films on other substrates have been proposed as optically implemented temperature sensors that are again limited via their multimaterial designs [20,21].

[1]Nuonics, Inc., 1862 Royal Majesty Court, Oviedo, FL 32765.

Manuscript received March 5, 2009; final manuscript received June 2, 2009; published online March 3, 2010. Review conducted by Allan Volponi.

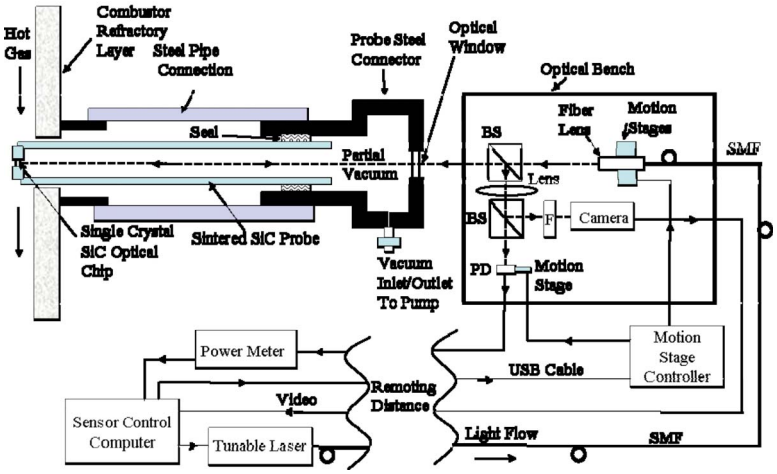

Fig. 1 All-SiC front-end probe-based optical sensor system for extreme gas temperature measurements in combustion engines

Given the mentioned challenging conditions, recently proposed is a temperature sensor innovation [22–29] that circumvents the inherent limitations of prior works. The fundamental design innovation involves three novel aspects. First, a single material is used to form the front-end probe, in our case, the material is SiC. By doing so, one places the vital SiC optical chip for temperature sensing within a SiC packaging tube, thus providing a CTE-matched materials scenario that is ideal in handling extreme temperature, pressure, and chemical conditions. Second, a freespace laser beam that forms a noncontact life-time reliable temperature reading mechanism is used to thermally isolate the temperature sensitive optics from the hot probe. In this way, the prior-art life-time limited wire conduit (electrical or fiber-optical) that transports the temperature information to the temperature reader (e.g., Volt-meter in the case of TCs) is eliminated. Third, active alignment fiber-optics with vacuum sealing of tube is used to target the hot chip within a confocal microscope geometry, thus forming a robust operation probe that combines the best of laser (wireless) and fiber (wired) remoting via a hybrid optical design solution.

2 Sensor System Design

Figure 1 shows the basic research design and method of the proposed all-SiC front-end probe sensor system used for extreme gas temperature measurement within the combustor section of a gas turbine. The system is subdivided into three thermally isolated subsystems forming a hybrid optical design engaging both wired and wireless optics. The first subsystem represents the sensor controls and processing station that is remotely located at a safe site for human interface. This subsystem includes the sensor control computer, optical power meter, and tunable laser. The remoting distance depending on the electrical signal drive requirements and can range from tens of meters to near a hundred meters. The second subsystem consists of the optical transceiver module containing targeting light beam and detection optics, active mechanics, and electronics. This transceiver module is located in close proximity (e.g., a few centimeters) from the front-end probe that forms the third subsystem that is uniquely passive, i.e., contains no lasers, detectors, electronics, or other electrically controlled device. The physical link between the controls subsystem and the transceiver subsystem is via one single mode fiber (SMF) optical cable and three electrical (USB style) cables, providing significant environmental isolation between the two sites. More importantly, the hot front-end probe subsystem is thermally decoupled from the transceiver subsystem with the only physical connection established via a single wireless optical link interfacing the hot SiC optical chip with the laser beam emerging from the SMF-coupled fiber lens (FL). The transceiver module is preferably enclosed in an environmentally protected chamber to minimize moisture, dust, and air currents. The transceiver module is designed for under 70°C operation that is ideally compatible with turbine manufacturer external safety and technician operational environment requirements. Furthermore, this friendly $<70^\circ$C temperature range is also compatible with temperature limits for standard fiber-optics, mechanics, and electronics. The transceiver module is mechanically interfaced to a thermally isolated cooler part of the turbine housing. The front-end probe subsystem consists of a steel connector that forms a pressurized fitting at the inlet to the engine combustor section, where gas temperature sensing is desired. This steel connector via a high temperature pressure seal connects to a long all-SiC probe that extends slightly into the hot gas section of the combustor. At the tip of this probe is embedded a thick single crystal SiC optical chip packaged within the sintered SiC material thus forming the much desired CTE-matched front-end. As shown, a steel pipe is used as an interface assembly between the probe steel pressurized connector and the hot gas section within the thermally isolating refractory layer. The probe steel connector has a high temperature window through which the laser beam travels but equally important, the connector has a vacuum inlet/outlet that connects to an on-demand vacuum pump. Maintaining a partial vacuum within the front-end probe structure is a critical innovation as it essentially eliminates laser beam turbulence along the long thermal ramp influenced probe path that, due to air currents within probe, can ruin beam alignment between chip and the FL. Furthermore, the partial vacuum prevents the unwanted convection-based cooling of the SiC optical chip from within the probe cavity. In addition, the presence of a vacuum cavity eliminates elevated temperature oxidization of the SiC sensor chip and the sintered SiC probe internal structure. Although Fig. 1 shows a single refractory layer between the hot gas section and the inlet to the combustor where the probe connector is attached (the scenario for our experiment), a typical deployed commercial combustor has several (e.g., >5) thick refractory layers such that there is a gradual temperature gradient between the extremely hot (say 1500°C) gas section and the probe insertion point where temperatures are under 200°C. Keeping the overall system design as three independent subsystems improves system maintenance efficiencies as repairs can be made by independent removal of subsystems, in particular, the front-end probe that will suffer the most from the harsh environment of the gas turbine.

The sensor system operates as follows. The computer controls

the required wavelength and power of the laser, as well as providing control signals for the remote motion controller. The computer also stores the received optical power readings for the given wavelength, as well as the received infrared (IR) beam video images from the alignment camera. To measure the gas temperature, the computer instructs the laser to provide optical power of a given infrared wavelength (e.g., 1550 nm) and amount (e.g., 10 dBm) to the SMF that in-turn feeds the FL operated in the low freespace-SMF coupling loss self-imaging condition between SiC chip plane and FL [30]. This light is launched toward the SiC chip sitting at the tip of the probe. The IR beam position at the SiC chip plane is electronically manipulated using piezo-actuators that control the FL translational and tip/tilt conditions such that the IR beam strikes after passing through the first beam splitter (BS) and optical window strikes the SiC chip for optimal retroreflection. Using the first BS coupled with another second BS, the SiC chip reflected light is routed toward two separate optical detection optics. A lens is used to produce focused beam spots on both the two dimensional (2D) camera, e.g., charge-coupled device (CCD) and the large area point photodetector (PD). The PD is also translated in unison with the FL controls such that the spot stays aligned on the PD active area. The computer processes the optical power and CCD image data and provides feedback control signals to the motion stage controller to adjust the optics for optimal interrogation of the SiC chip. The infrared band filter F (e.g., bandwidth of 1530–1560 nm) blocks the black-body (BB) radiation produced by the SiC optical chip that is captured by the lens optics, thus allowing only the laser beam to pass through to the CCD, and hence preventing camera saturation. In short, the sensor system operates to actively target the SiC optical chip and then to properly recover the received retroreflected temperature coded beam to deduce the SiC chip, and hence the gas environment temperature. The SiC chip acts as a temperature sensitive Fabry–Pérot (FP) cavity and previously described multiwavelength signal processing techniques implemented via the control computer can be used to deduce the optical chip temperature [23,26,28]. In short, the SiC chip reflected light optical power is given by the classic FP expression:

$$R_{FP} = \frac{R_1 + R_2 + 2\sqrt{R_1 R_2}\cos\varphi}{1 + R_1 R_2 + 2\sqrt{R_1 R_2}\cos\varphi} \tag{1}$$

where $\varphi = 4\pi/\lambda n(\lambda, T)t(T)$. Here $n(\lambda, T)$ is the chip refractive index at wavelength λ, T is the chip temperature, $t(T)$ is the chip thickness at temperature T, and R_1 and R_2 are the classic Fresnel power coefficients for the SiC-air interface given by $R_1 = R_2 = [(1-n)/(1+n)]^2$. Do note the SiC chip is of a thick (e.g., 400 μm) single crystal SiC material that is optically flat and mechanically robust for handling high (e.g., 160 atm) pressures [23] and high temperatures (e.g., 1500°C). The SiC material that makes the chip and front-end probe is also robust to chemical attack with excellent thermal properties for handling extreme temperatures [25].

3 Sensor Assembly and Experimental Turbine Rig Test

Figure 2 shows the Nuonics, Inc. (Oviedo, FL) provided all-SiC front-end probe displayed in its unassembled and assembled fashions. The point to note is the harsh environment front-end probe assembly consists of three parts, namely, (a) the all-in-one SiC probe consisting of sintered SiC tube assembly with an embedded single crystal SiC optical chip, (b) the pressure sealed steel connector housing that the probe is inserted into to form an interface with pressurized turbine chamber, and (c) the connector flange with an optical window and vacuum connection housing that can connect to the vacuum pump. The probe uses a 400 μm thick single crystal SiC chip of 1×1 cm^2 size embedded with a nonporous sintered SiC tube of 41.5 cm length, and 2.1 cm and 3.3 cm inner and outer diameters, respectively. The pressure seal between the sintered SiC tube and the steel connector is of Viton material with a maximum sealing temperature of 205°C. The window (with 3 deg wedge angle) is made of a 2.54 cm diameter and 6.35 mm thick magnesium fluoride (MgF_2) material with a specified high temperature handling of 500°C and 800°C in moist and dry conditions, respectively. The wedge design eliminates interference effects from the window acting as a wavelength and temperature sensitive cavity. A Mityvac model EW-79301-20 hand operated vacuum pump is connected to the probe vacuum valve and a 25 in.-Hg (~85 kpa) partial vacuum is established within the probe. A cold test of the probe indicates a vacuum drop to 19 in.-Hg and 2 in.-Hg after 62.5 h and 240 h (10 days), respectively. The probe is thermally treated over 30 thermal treatment cycles using an oven with a room temperature (~20°C) to 1100°C thermal cycle consisting of a ramp up time of 4.5 h and cool time of 12 h.

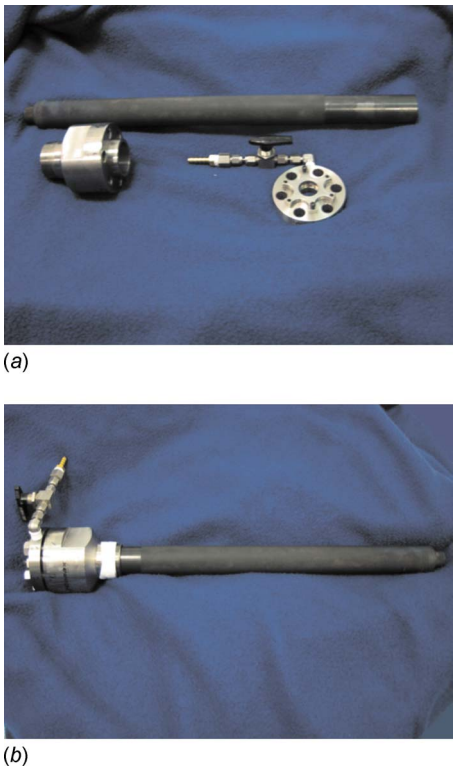

(*a*)

(*b*)

Fig. 2 SiC temperature front-end probe shown in an (*a*) unassembled and (*b*) assembled fashion

Next, the described all-SiC front-end probe along with its Fig. 1 transceiver is deployed in a Siemens (Orlando) combustion test rig facility (see Fig. 3) to form an industrial scenario gas turbine temperature sensing system for a proof-of-concept industrial harsh

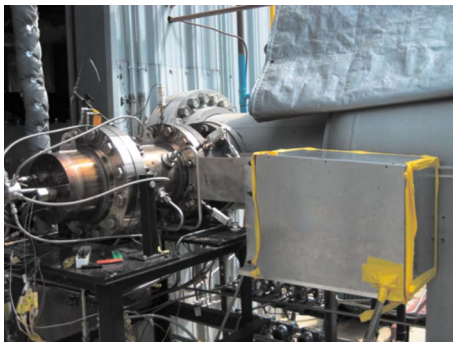

Fig. 3 All-SiC temperature sensor deployed for a first test at Siemens rig facility

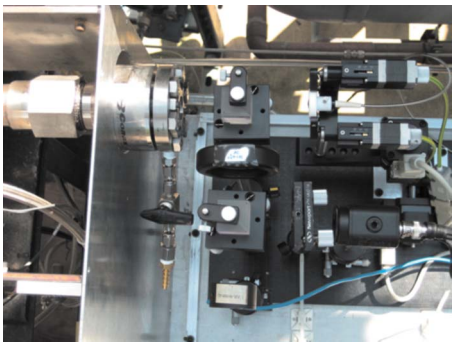

Fig. 4 The assembled sensor optical transceiver module top view

environment sensor technology test. The test combustor is engaged with six 30 cm long reference type-B platinum–rhodium TCs with ceramic and platinum sheath shields for protection and support and a $\pm 0.25\%$ uncertainty, and 1 s response and data recording time. In addition, the all-SiC probe is located in the combustor exhaust section in close proximity (within ~ 14 cm) to the TCs that are located at the midsection of the combustor. A 23 cm length of each TC sits within the combustor encasing while a 5 cm length of the SiC probe sits within the hot section of the combustor. The 35.5 cm(length) $\times$ 20 cm(width) transceiver optical bench is boxed in a water proofed 48 cm(length) $\times$ 30 cm(width) $\times$ 37.5 cm(height) aluminum housing that includes a moisture absorbing desiccant bag to counter the rainy high humidity weather in Florida. The housing is also earthed to counter the lightening strikes common in Florida.

The bench optical layout (see top view in Fig. 4) distances are as follows. Fiber lens to first BS: 5.25 cm; fiber lens to SiC optical chip: 60 cm; first BS to probe window: 6.25 cm; first BS to focusing lens: 5 cm; lens to PD: 11.25 cm; lens to camera: 15 cm. The focal length of the lens is 10 cm. Beam diameter size of 0.8 mm is detected on CCD with <0.8 mm diameter beam on the PD. The PD is a Newport model 818-IR large 3 mm diameter active area point detector, while the BB radiation reduction filter F is centered at 1550 nm with a 30 nm (full-width half-max) passband. The camera is a video rate IR 2D CCD, while Standa piezoelectric translation and tip/tilt motion stages are used to optimize beam alignment. A laser spot size of 550 μm $1/e^2$ beam size forms on the SiC chip. The test rig and control room hardware are connected via 15 m of one SMF and three 10 m electrical cables. The control room contains other rig operational systems such as TC and pressure data reading electronics, as well as combustor flame and fuel monitoring systems. The probe passes through a single 7.62 cm thick combustor refractory layer that for a sample test indicated an external refractory temperature of 426°C when the combustion chamber maximum gas temperature reached 1370°C, indicating the large (in this case, 944°C) temperature drop and high intrinsic thermal insulation of the deployed refractory.

The rig operation begins with an initial warm-up and operational check period, when the hot air blowers are turned on and the combustor is pressurized to a desired ~ 100 psi (or 7 atm) as shown in Fig. 5. For the performed hot rig tests, this warm-up time varied greatly due to various changing on-ground rig conditions and ranged from 20 min to 5 h. Once the rig has reached stable warm-up operational conditions with a fuel-air ratio ~ 0.05, the combustor flame is lit. At this stage, the combustor flame ignited localized gas temperature drastically ramps up over a 1000°C in ~ 3 s. In effect, the entire combustor and all its inserted temperature measuring instruments suffer a great thermal shock. In our case of first rig flame lighting, one reference TC completely failed (no electrical signal out), while another gave drastically wrong temperature readings. The remaining four TCs continued to supply appropriate temperature readings to the remote data acquisition system. This unwanted behavior of these high performance type-B TCs was expected, and hence six TCs were deployed for redundancy. The all-SiC probe survived the thermal shock as optical data readings from both the PD and IR CCD continued to register. In fact, the CCD camera recording at the video rate of 30 fps produced a rapid sequence of an on/off blinking laser spot (see Fig. 6) that spatially darted around a 1 mm diameter around the original alignment point before settling to a beam position within 0.25 mm diameter from its original spot on the camera. The darting around is due to the thermal shock the probe front-end suffers on flame ignition causing the SiC chip surface to temporally deform causing the retroreflected beam to misalign from its original on-axis position of the camera. In addition, the flame ignition also slightly misaligns the probe mechanical assembly causing the retroreflected beam to be slightly off its cold alignment position. Nevertheless, both dynamic and settled beam positions stay within the 3 mm diameter active area of the PD, and furthermore are well within the CCD image zone to allow

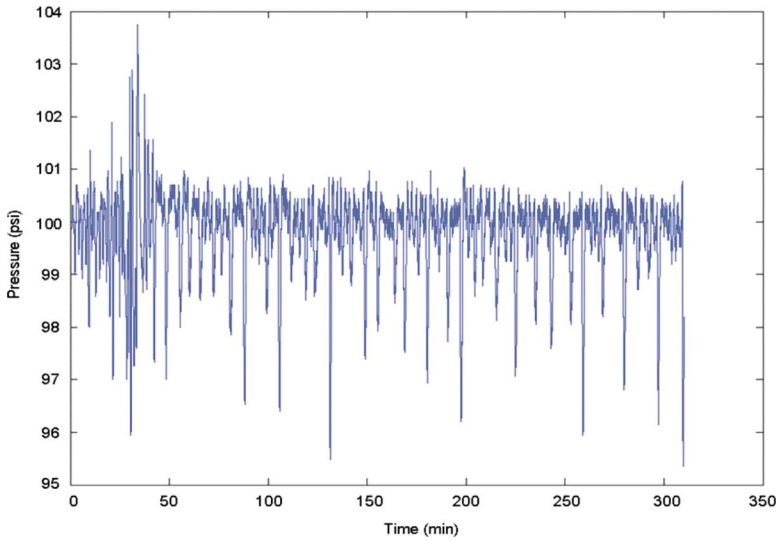

Fig. 5 Combustor average pressure readings of ~ 100 psi (7 atm) measured during rig operations

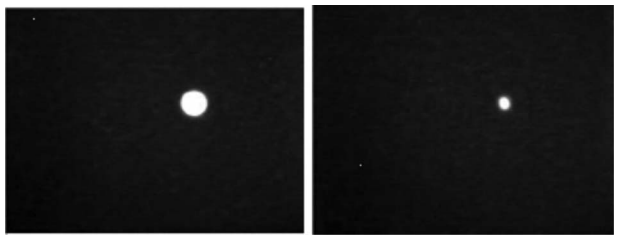

Fig. 6 IR CCD camera (8.8×6.6 mm² active area view) received laser beam snap shots during thermal shock stage indicating on/off oscillatory Fabry–Pérot étalon behavior of SiC optical chip due to the rapid thermal gradient. Left photo: power max and right photo: power min.

the piezo-actuators to optimize beam alignment. The PD's power meter coupled to the control computer is set to take optical power readings after every 78 ms. After the flame light-up, the rig gas temperature near the TC after a ~23 min time interval (see TC data) settles into its expected high temperature operational range with measured TC maximum temperatures reaching 1239°C. Do note that for this particular test rig, one could not set or stabilize the combustor to a given high temperature; thus each time the rig is operated, one finds the combustor temperature sitting in a range between 1100°C and 1239°C.

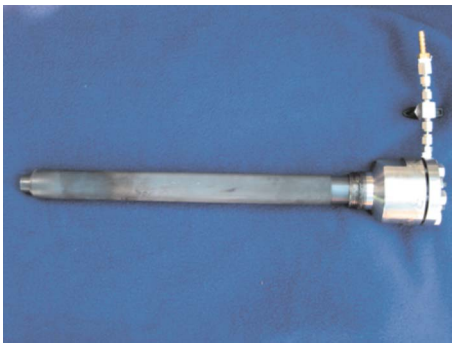

Fig. 7 After first rig test of probe, expected part front-end discoloration is seen due to chemical exposure in combustor refractory section

4 Rig Test Results and Discussion

Over a 28 day period, the probe was subjected to combustor operations on 6 days, with each given day the combustor turned on and then off after test operations. After the first rig test, the probe is removed from the rig and inspected for optical and mechanical failures. The probe showed no damage apart from some expected discoloration (see Fig. 7) of part of the front-end due to chemical treatment in the hot soup of the combustor refractory zone. The probe is reinserted into the system to continue rig test operations.

Figure 8 shows the raw optical data provided by the PD for one of the test days. For the same test, Fig. 9 shows the equivalent temperature readings provided by one of the four working TCs in the rig. Both TC and PD data acquisition systems are synchronized via a computer clock's locked time counter, so one can have direct one-to-one mapping of probe optical power to TC measured temperature to enable probe calibration. Ideally, the optical probe must be calibrated using a temperature measuring device that has far better measurement accuracy than today's high temperature TCs. In addition, the probe calibration must be done at a much slower temporal rate versus an uncontrolled thermal shock mechanism of the rig.

One can clearly see the expected Fabry–Pérot effect oscillatory behavior of the optical power during thermal ramping. In addition, the optical power picks up an increasing bias level due to increasing BB radiation during ramping. In addition, the optical power continues to oscillate depending on the rig temperature fluctuations at the set higher temperature zone. This is so as the optical sensor is designed to be sensitive to high temperature zone changes in a 20°C increment indicating that optical power goes from a peak to a null if temperature changes by 10°C. This feature points to the fact that the optical sensor can measure temperature to a very high accuracy given the optical power meter is highly sensitive.

Figure 10 shows a 15 min snap shot of the probe optical power data taken in the stable ~1107°C region of the rig operation. This data indicates that the probe temperature measurement standard

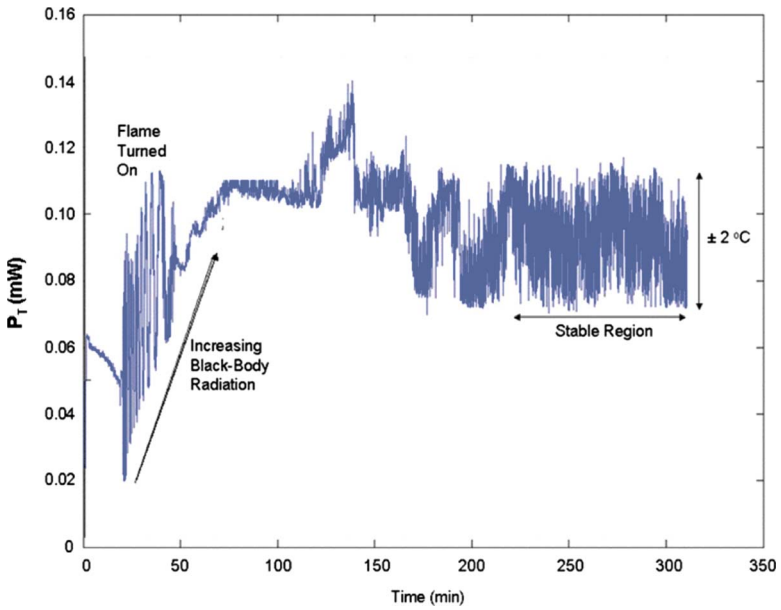

Fig. 8 Raw optical data recorded by the probe PD indicating the rig thermal ramp zone and the relative high temperature stabilization zone. Vertical axis is measured optical power in mW and horizontal axis is a time counter.

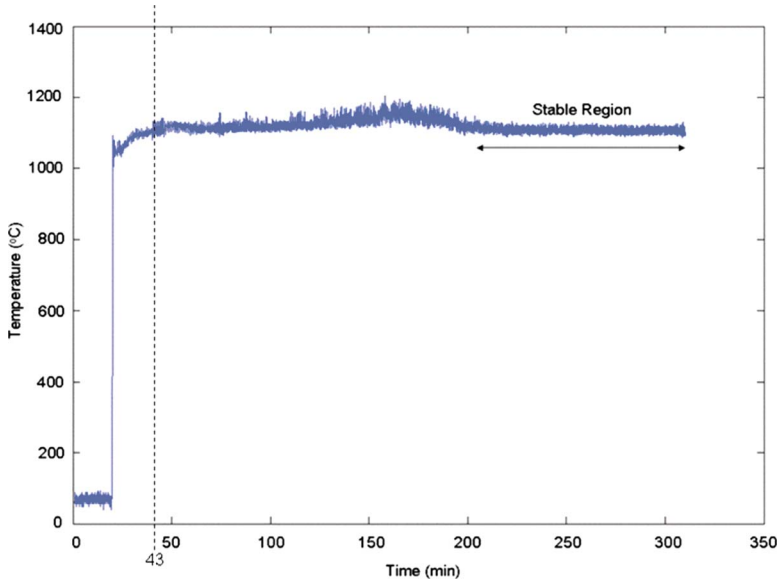

Fig. 9 Rig TC provided temperature reading during the Fig. 8 optical data acquisition period. This TC data is used for optical probe calibration. Vertical axis is measured temperature and horizontal axis is a time counter. A 43 min marker line indicates when the rig gas temperature near TC settles down in its high temperature range that is 23 min after thermal shock.

deviation (SD) is ±2°C for time snap shots of 30 min, 15 min, and 1 min sections. Given the deployed power meter accuracy of 1 μW, the given optical sensor has a calculated sensing accuracy of 0.18°C. Figure 11 shows the Fig. 10 data of 15 min time period TC data. This TC data indicates temperature measurement SD of ±8.3°C, ±8.1°C, and ±9.9°C for time snap shots of 30 min, 15 min, and 1 min sections, respectively. Given that the TC indicates an averaged temperature of 1107°C, the specified TC measurement accuracy for this data is ±2.8°C, indicating a possible limitation of TCs compared with the proposed optical probe that has the potential to deliver much better measurement resolution.

BB radiation fundamentally depends on Planck's law that relates the amount of BB radiation to the temperature of the BB source and the wavelength of radiation and is given by:

$$L_b(\lambda, T) = \frac{C_1}{\pi\lambda^5}\frac{1}{e^{C_2/\lambda T} - 1} \tag{2}$$

where $L_b(\lambda, T)$ is the spectral radiance, λ is the wavelength of radiation, T is the temperature of the BB, while C_1 and C_2 are radiation constants given by $C_1 = 2hc^2$ and $C_2 = hc/k$. The total amount of BB radiation is given by the area under the spectral radiance versus wavelength curve. As the temperature increases the peak of this curve moves to higher intensities and shorter wavelengths, resulting in an increase in the total amount of BB radiation. The actual amount of BB radiation detected depends on the wavelength response of the PD used.

Fig. 8 optical data after the flame light-on region indicates that the rig cavity, and hence the optical probe take a considerable time

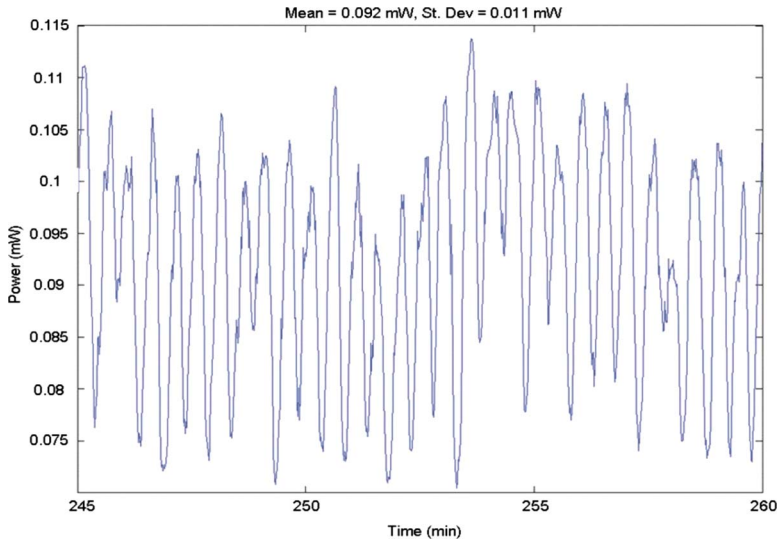

Fig. 10 15 min snap shot of optical power readings from probe during the stable ~1107°C region of the rig operation with a standard deviation of ±2°C.

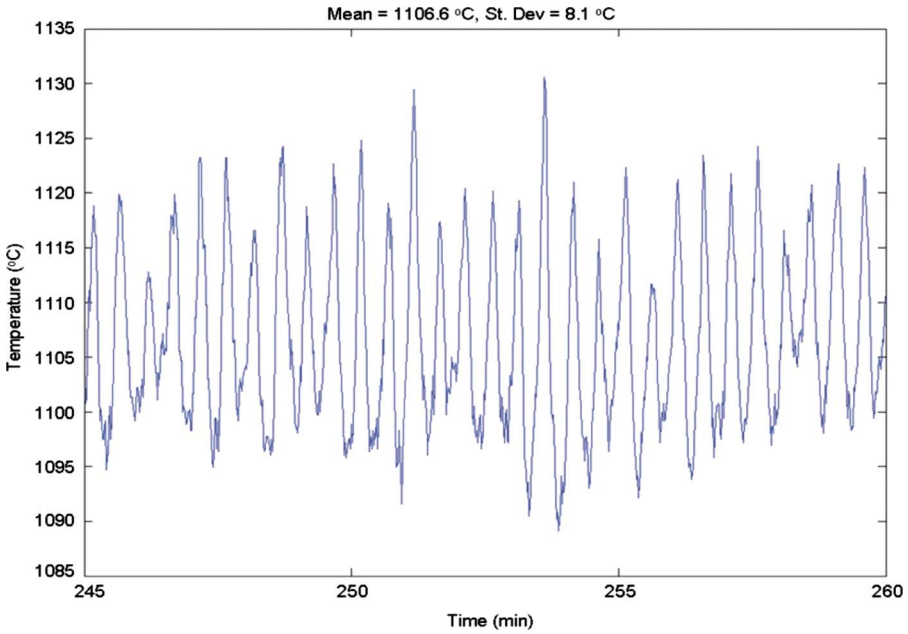

Fig. 11 TC data during the Fig. 9 data 15 min time period with a standard deviation of ±8.1°C

after thermal shock to give stabilized PD-based optical power readings. This is mainly due to the fact that the presently designed all-SiC probe has a partial externally exposed SiC chip optical window that allows BB radiation from the rig hot copper internal walls to pass through the probe cavity in-line path to the PD optics. As the combustor rig is a large BB radiation cavity, a significant time of 48 min after thermal shock is taken for the entire rig to reach the stable high temperature given by its increasing BB radiation signature, thereby producing a slow build-up of the PD optical power data shown in Fig. 8. Note that compared with the TC that is mostly encased within the combustor, the SiC probe generates a large thermal mass due to its large highly conducting (thermal) heat sink structure that at present mostly sits outside the hot zone of the combustor. In effect, the probe thermal mass due to its physical size and nonoptimal single refractory layer placement in combustor limits the dynamic response of the probe temperature measurement. One can note that once the rig has reached its stable high temperature, the optical probe is quick to pick up small temperature changes. Nevertheless, the mentioned probe thermal mass at present has a clipping effect on the actual temperature readings, where the shown ±8.1°C TC readings are clipped to ±2°C probe temperature readings. The solution for reducing this current experimental probe performance limitation is to reduce the probe thermal mass by (a) placing most of the SiC probe within the combustor section including within the highly insulating refractory layers that is typical of a deployed combustion turbine and (b) to design a physically smaller sintered SiC probe package with slow thermal sinking between the SiC optical chip and the sintered SiC probe package. Do note that in the thermal shock region, the all-SiC optical probe did respond in real-time (or video rate) indicated by the rapidly pulsating on/off laser beam images with a 33 ms video time interval.

Fig. 12 shows the optical probe measured temperatures over the whole duration of the rig operation. The signal processing method to find the Fig. 12 temperature plot using the Fig. 8 optical probe data is detailed in the Appendix. The Fig. 12 curve shows that the stable region average temperature of the gas in the rig is 1107°C and the SD in the indicated 60 min stable region is ±6.3°C and ±2°C given by the TC and SiC probe, respectively. Do note that to ensure high temperature measurement sensitivity around the detected laser power maximas and minimas, the optical probe can be calibrated for a second slightly different wavelength that would ensure that for any given temperature, the received laser power reading for at least one of the two calibration wavelengths is in the highly sensitive region for laser power-based temperature signal processing. Fig. 13 shows data from the Fig. 12 zoomed in region around the thermal shock time zone indicating that the measurement response of the TC is under-damped, whereby it oscillates around the temperature of the gas. In contrast, the temperature measurement response of the optical probe is heavily damped, whereby after a fast initial response due to thermal shock, the response slowly (in ~16 min) approaches the temperature of the gas (see Fig. 13). Assuming that the heat is transferred from the hot gas to the TC or the optical probe at an exponentially slow rate (a valid assumption for convective heat transfer thermal systems [31]), thermal time constants can be determined to give a measure of the thermometer response time τ. Hence, one can write measured elevated temperature $T(°C)=[T_f-T_i][1-\exp(-t/\tau)]+T_i$, where T_i and T_f are the initial and final temperatures, respectively.

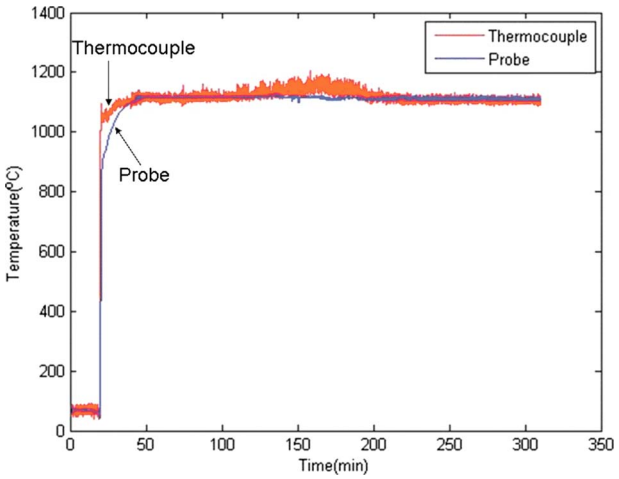

Fig. 12 Comparative optical probe and TC measured temperatures over the duration of the rig operation

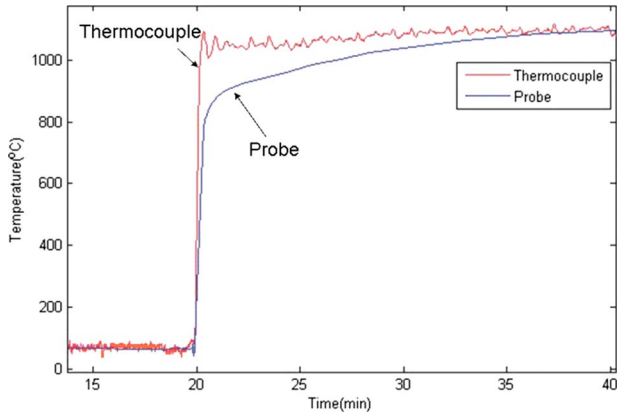

Fig. 13 Comparative optical probe and TC measured temperatures over the zoomed in thermal ramp duration of the rig operation

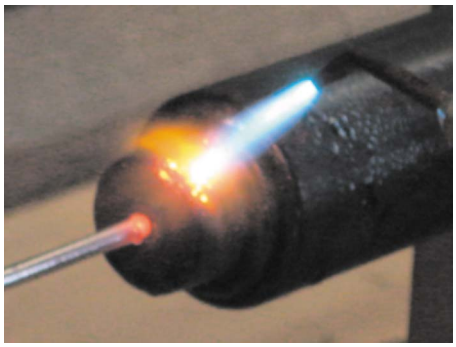

Fig. 14 All-SiC probe and type-R high temperature thermocouple under oxyacetylene flame thermal and localized thermal ramp joint test with temperatures reaching 1600°C

Using Fig. 13, a thermal time constant of 10 s is computed for the TC as this is the time it takes for the TC to reach 63.2% (or 1–1/e) of the difference between the thermal ramp start and end temperatures or for $T=0.632\cdot(1050-87)+87=695°C$. In comparison, using Fig. 13, the thermal time constant for the all-SiC probe is computed as a TC comparable 18 s. As mentioned earlier, this limited dynamic temperature measurement response of the SiC probe owes its behavior to the probe's large thermal mass via its present physical size and its current nonoptimal thermal refractory insulation experimental conditions. Nevertheless, the present rig test of the proposed all-SiC probe technology has proven its operational robustness in the harsh conditions of a commercial test combustion rig.

Specifically, Table 1 shows the conducted key operational parameters for the probe rig test. For example, the probe survived eight thermal up-ramps of 1000°C, each ramp of ~3 s. The probe also survived localized thermal shock (see Fig. 14) and maintained mechanical integrity when subjected to an oxyacetylene flame that produced temperatures near 1600°C. In fact, the R type thermocouple began to melt using the oxyacetylene flame setup, while the all-SiC probe stayed intact. It is important to note that the on/off modulation depth of the retroreflected signal off the SiC optical chip varied from 20:1 to 2:1 during the 28 days of rig tests as different parts of the external chip zone were optically spoiled to a different degree by the hot chemical soup in the combustor. Using the active beam alignment system in the probe, one was highly effective in finding a high modulation depth spot on the chip for effective optical power data recording, again proving the versatility of the smart beam targeting probe design when operating under harsh conditions of a commercial gas turbine. As the optical power meter is highly sensitive, even a 2:1 optical power ratio between a 10°C temperature change provides significant signal processing resolution to calculate the measured temperature with high (e.g., 0.2°C) accuracy.

The probe operated successfully for 28 days, eventually developing a vacuum seal breakage (see Fig. 15) in the pressurized connector on the lower temperature side of the probe. This led to unwanted combustor cooling water entry into the probe at high temperatures (~1200°C) and stoppage of probe operations. A higher (>200°C) temperature insulating pressure seal needs to be deployed to prevent seal breakdown. Do note that during operations, the temperature of the external part of the probe steel connector registered a 200°C reading, indicating that heat from the combustor was efficiently traveling via the probe structure to the external connector chamber. This can indeed be prevented in a deployed combustor using many more thermally insulating refractory layers between probe front-end and connector zone. This would lead to a much lower connector external temperature, and also a much lower temperature experienced by the Viton seal in the connector. In addition, the thermal mass of the probe would be greatly reduced thereby improving the dynamic temperature measurement response of the probe.

Figure 16 shows the probe condition after 28 continuous days in the rig. One can notice the (blue) copper sulfate deposits on the probe front-end. This is indeed so as the combustor chamber was made from copper and the cooling water had sulfur content in it.

5 Conclusion

To our knowledge, for the first time, a single material front-end temperature sensing probe using sintered and single crystal forms of SiC has been assembled and tested in a combustion rig. The probe features a hybrid optical design using a standard silica fiber in the cooler section and a thermally isolated wireless optical link that engages the hot section of the combustor. The probe showed mechanical robustness, surviving eight near 1000°C over 3 s thermal shocks during flame lightings. The probe provided the appropriate optical signal for temperature sensing and signal processing with rig temperatures reaching 1200°C. As the rig operated with greatly reduced thermal refractory layers that would otherwise be present in gas turbines, the deployed Viton gas seal in the probe assembly was exposed to elevated temperatures above the 200°C seal design temperature, thus leading to seal damage and gas leakage into the probe. Rig operations indicate that the SiC chip optical response of the direct gas exposed zone is affected by the combustor dirt; nevertheless, the chip zone within the probe assembly that has surface protection continues to provide a strong

Table 1 Summary of all-SiC probe test at Siemens rig

Combustion rig flame active operation	6 days
No. of times probe experienced flame light and thermal shock (temperature ramp of 1000°C in 3 s)	8 (1 day, 3 flame lights, 5 days, 1 flame light/day)
Operation with flame on	26 h
Operation with flame off and blower on	13.5 h
Number of combustion heat and cool cycles	8
Days in external rig environment	28 days

Fig. 15 Condition of Viton seal used in the probe connector before and after 28 days in rig

optical signal. The probe also survived several localized thermal shocks of 1600°C using a flame torch. Future work requires probe front-end redesign for optimal chip protection with direct signal processing and probe miniaturization and appropriate placement in combustor to reduce thermal mass and improved probe temporal response. Unlike EMF-based TCs used for extreme temperature sensing, the proposed probe does not suffer from the intrinsic limit of temperature measurement error being a percentage of the temperature measured. In addition, unlike TCs, the probe front-end is a single material package, thus pointing to the promise of the proposed all-SiC temperature probe technology for gas turbine extreme temperature sensing.

Acknowledgment

This paper was prepared with support of the U.S. Department of Energy. Equipment and design support was provided by Nuonics, Inc., including the Nuonics SiC temperature probe. Part of the paper describes work conducted at Nuonics, Inc. with collaboration from Siemens Power Generation, Orlando, FL. The authors also thank S. Azer Reza of PIPS Lab. UCF for experimental support, and R. Bunce, D. Sheldon, and Dr. N. Ulerich of Siemens for rig support.

Appendix: Measuring Temperature via Probe Raw Photodetector Data

The raw photodetector data P_T (Fig. 8) contains both BB radiation P_{BB} and laser reflected power P_L off the SiC chip leading to the expression:

$$P_T = P_{BB} + P_L \tag{A1}$$

Equation (A1) can be further written in terms of its dc or $P_{T(dc)}$ and ac or $P_{T(ac)}$ components giving

Fig. 16 Probe condition showing copper sulfate deposits after 28 continuous days in the rig (available in color online)

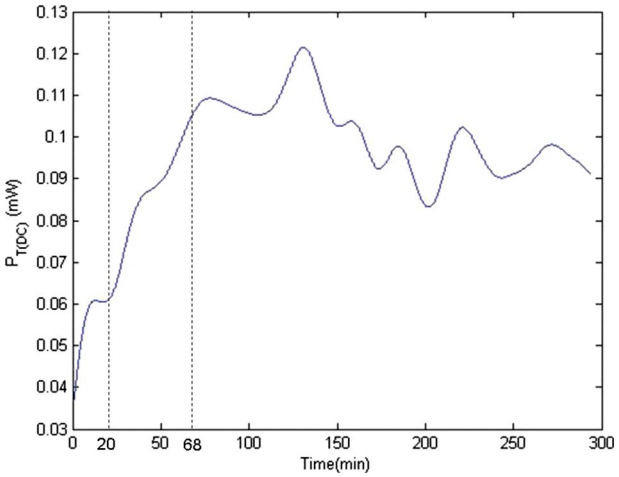

Fig. 17 Photodetector dc value $P_{T(dc)}$ generated from filtering P_T Fig. 8 experimental data against time

$$P_T = P_{T(dc)} + P_{T(ac)} \tag{A2}$$

Here, the dc and ac contributions to the total PD optical power came from both the laser and BB optical powers. The dc contributions of the total optical power due to BB and laser are given as $P_{BB(dc)}$ and $P_{L(dc)}$, respectively. Similarly, the ac contributions of the total optical power due to BB and laser are given as $P_{BB(ac)}$ and $P_{L(ac)}$, respectively. Hence one can write

$$P_T = (P_{BB(dc)} + P_{L(dc)}) + (P_{BB(ac)} + P_{L(ac)}) \tag{A3}$$

One can further write

$$P_{BB(ac)} + P_{L(dc)} + P_{L(ac)} = P_T - P_{BB(dc)} \tag{A4}$$

Since $P_{BB(ac)} \ll P_{L(ac)}$ for the given experimental conditions in the stable region of the present rig temperature measurement scenario (e.g., for a 10°C change at 1100°C, P_L changes by 70 μW, while P_{BB} changes by 8 μW, Eq. (A4) can be approximated as

$$P_{L(dc)} + P_{L(ac)} \approx P_T - P_{BB(dc)}$$

$$P_L = P_T - P_{BB(dc)} \tag{A5}$$

Note that P_L can be used to find the SiC probe tip temperature, and hence the gas temperature at or near the probe tip. P_L is determined by subtracting $P_{BB(dc)}$ from P_T. To determine $P_{BB(dc)}$ shown in Fig. 17, first $P_{T(dc)}$ is determined by passing the Fig. 8, P_T data through a computer implemented low-pass filter. The low-pass filter used is a 5th order type Butterworth filter with an angular cutoff frequency of 0.005π rad/sample or equivalently, 0.2 rad/s, since the power readings are taken 78 ms apart.

Note that the BB radiation compared with the laser power is significant only for temperatures >700°C in the present experimental scenario (at 700°C, the BB radiation is 7.5 μW compared with the average laser power of 57 μW determined from the complete min/max cycles that occur just after the thermal ramp. This is consistent with Planck's black-body radiation law (Eq. (2)), according to which the black-body spectrum shifts to lower wavelengths and higher powers as the temperature goes up. Hence, one can assume that before the thermal ramp at the 20 min timer mark, $P_{BB(dc)}=0$. After the near 3 s flame lit thermal shock at the ~20 min time marker, the entire rig and its internal constituents (e.g., gas soup, SiC probe, TCs, and combustor copper wall) experience thermal ramps. In turn, $P_{T(dc)}$ starts to increase, and this increase is entirely due to BB radiation. This is because

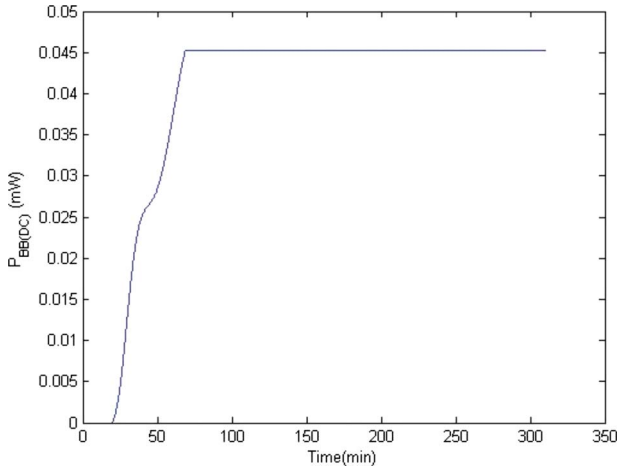

Fig. 18 Clamped photodetector dc value $P_{BB(dc)}$ against time after considering received laser power max/min swing

the thermal shock causes the laser power to rapidly go through many rapid complete power max/min cycles that leads to $P_{L(dc)}$ remaining a constant level.

The max-to-min laser power P_L swing is determined from the complete min-to-max P_T cycles that occur just after the thermal ramp (see Fig. 8), when there is no BB radiation (i.e., when temperature $<700°C$) and gives a P_L swing of 75 μW with $P_L(\text{minimum})=20$ μW and $P_L(\text{maximum})=95$ μW. Since the maximum value of P_T recorded is 140 μW after the thermal ramp settles (see Fig. 8), it implies that the $P_{BB(dc)}$ can be no smaller than 45 μW in the stable temperature region after the thermal ramp. Similarly, the minimum value of P_T recorded is 70 μW after the thermal ramp settles, which implies that the $P_{BB(dc)}$ can be no larger than $70-20=50$ μW in the stable temperature region after the thermal ramp. Within this range, i.e., 45–50 μW, a $P_{BB(dc)}$ value of 45 μW that occurs at the 68 min time marker in Fig. 8 is picked as that conforms most to the P_L max/min cycles occurring nearest to the stable temperature region. To implement signal processing for temperature measurement, $P_{BB(dc)}$ data in Fig. 17 are clamped to its value at the 68 min mark to produce Fig. 18, as 45 μW is the value $P_{BB(dc)}$ can reach if one assumes that the laser power P_L completes a max-to-min swing subsequently.

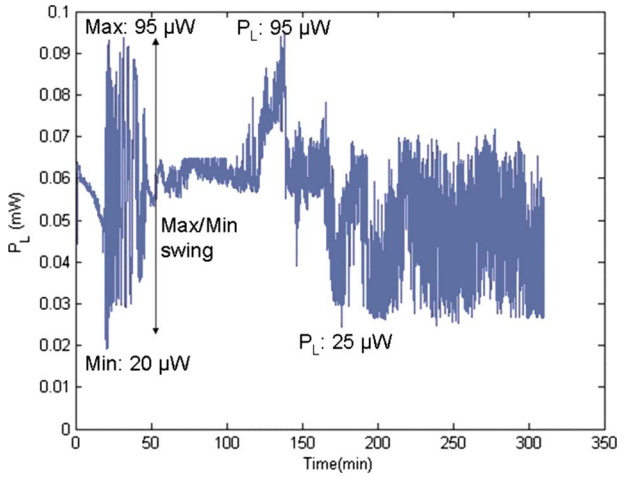

Fig. 19 Computed laser power P_L from raw power P_T data using Eq. (A5) and plotted against time

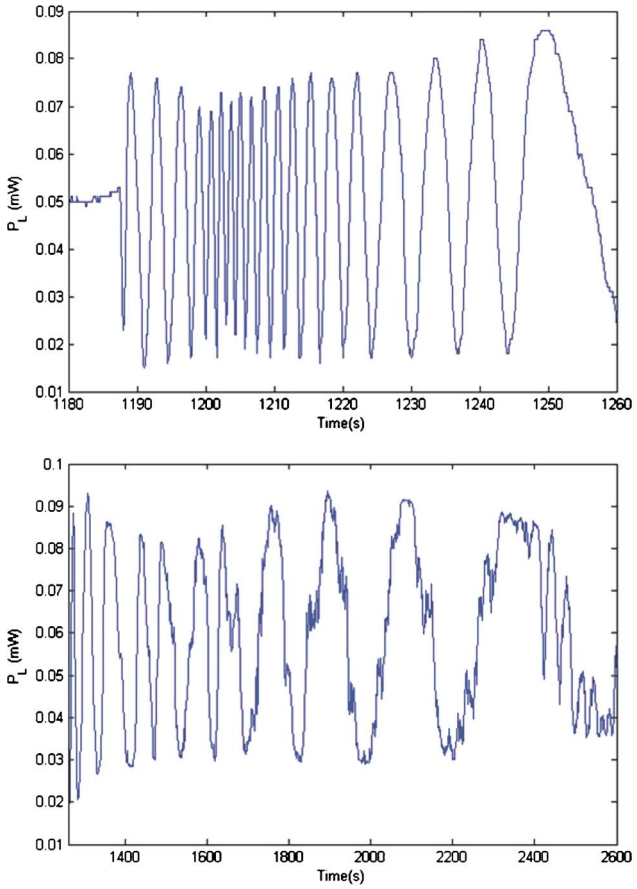

Fig. 20 Zoomed in versions of Fig. 19 around the thermal ramp region

As the temperature of the combustor rig given by the reference TC does not change by much (i.e., it fluctuates around 1120°C) after the 68 min time marker, $P_{BB(dc)}$ is taken to be constant value of 45 μW after this time instant. As $P_{BB(dc)}$ is now determined, P_L is simply determined according to Eq. (A5) to produce the Fig. 19 P_L data.

Near the probe tip, the all-SiC probe measured coarse temperature of the gas in a ~20°C range can be determined from Fig. 19 data by finding the number of laser power min-to-max cycles that have passed starting from the initial (i.e., time marker of zero) rig temperature (87°C) and comparing that to a previously calibrated laser power P_L against temperature probe calibration curve [23].

Figures 20(*a*) and 20(*b*) show the zoomed in snapshots of these P_L laser power cycles at different time instants after the flame ignited thermal shock. Within each 20°C window, the exact temperature is found by comparing the Fig. 19 actual power reading against the calibrated P_L curve to get the Fig. 12 probe provided temperature values. Note that the laser reflected power off the SiC chip varies with temperature according to Eq. (1).

References

[1] Pacala, S., and Socolow, R., 2004, "Stabilization Wedges: Solving the Climate Problem for the Next 50 Years With Current Technologies," Science, **305**(5686), pp. 968–972.

[2] Hoffert, M. I., Caldeira, K., Jain, A. K., Haites, E. F., Harvey, L. D. D., Potter, S. D., Schlesinger, M. E., Schneider, S. H., Watts, R. G., Wigley, T. M. L., and Wuebbles, D. J., 1998, "Energy Implications of Future Stabilization of Atmospheric CO_2 Content," Nature (London), **395**, pp. 881–884.

[3] Hawkins, D. G., Lashof, D. A., and Williams, R. H., 2006, "What to Do About Coal," Sci. Am., **295**(3), pp. 68–75.

[4] Langston, L. S., 2007, "Fahrenheit 3600: Everywhere You Look, The Gas Turbine Industry is Running Hot," ASME Mechanical Engineering Magazine, **129**(4), pp. 34–37.

[5] Manley, D. K., McIlroy, A., and Taatjes, C. A., 2008, "Research Needs for Future Internal Combustion Engines," Phys. Today, **61**(11), pp. 47–52.
[6] Bonafoux, J., 2004, "Propulsion System Requirements for High Speed Naval Ship Designs," RENK Symposium, Paper No. 42.
[7] O'Rourke, R., 2006, "Navy Ship Propulsion Technologies: Options for Reducing Oil Use-Background for Congress," Congress Research Service (CRS) Report No. RL33360.
[8] Ausubel, J. H., 2004, "Big Green Energy Machines," Ind. Phys., **10**(5), pp. 20–24.
[9] Bentley, R. E., 1998, "Thermocouple Materials and Their Properties," *Theory and Practice of Thermoelectric Thermometry: Handbook of Temperature Measurement*, Springer-Verlag, Singapore, Chap. 2, pp. 25–81.
[10] Ripple, D., 2000, "Thermocouples and Thermocouple Wires," Tutorial in NIST Thermocouple Workshop, IEEE Conference on Advanced Thermal Processing of Semiconductors.
[11] Lee, B., 2003, "Review of the Present Status of Optical Fiber Sensors," Opt. Fiber Technol., **9**(2), pp. 57–79.
[12] Winz, M., Stump, K., and Plant, T. K., 2002, "High Temperature, Stable Fiber Bragg Gratings," *Proceedings of the 15th Optical Fiber Sensors Conference Technical Digest (OFS 2002)*, p. 195.
[13] Grobnic, D., Smelser, C. W., Mihailov, S. J., and Walker, R. B., 2004, "Isothermal Behaviour of Fiber Bragg Gratings Made With Ultrafast Radiation at Temperatures Above 1000°C ," Opt. Commun., **2**, pp. 130–131.
[14] Hai, X., Wei, Z., Lockhard, R., and Anbo, W., 1997, "Absolute Sapphire Optical Fiber Sensor for High Temperature Applications," Proc. IEEE, p. 351.
[15] Grobnic, D., Mihailov, S. J., Smelser, C. W., and Ding, H., 2004, "Ultra High Temperature FBG Sensor Made in Sapphire Fiber Using Isothermal Using Femtosecond Laser Radiation," Opt. Commun., **2**, pp. 128–129.
[16] Zhang, Y., Pickrell, G. R., Qi, B., Safaai-Jazi, A., and Wang, A., 2004, "Single-Crystal Sapphire-Based Optical High-Temperature Sensor for Harsh Environments," Opt. Eng., **43**(1), pp. 157.
[17] Dewitt, D. P., and Nutter, G. D., 1988, *Theory and Practice of Radiation Thermometry*, Wiley, New York.
[18] Ng, D., and Fralick, G., 2001, "Use of a Multiwavelength Pyrometer in Several Elevated Temperature Aerospace Applications," Rev. Sci. Instrum., **72**(2), pp. 1522–1530.
[19] Bonzani, J. P. J., Florczak, E. H., Scire, J. J. J., and Markham, J. R., 2003, "Improvement to a Bench Top Instrument for Measuring Spectral Emittance at High Temperatures," Rev. Sci. Instrum., **74**(6), pp. 3130–3136.
[20] Beheim, G., 1986, "Fibre-Optic Thermometer Using Semiconductor-Etalon Sensor," Electron. Lett., **22**(5), pp. 238–239.
[21] Cheng, L., Steckl, A. J., and Scofield, J., 2003, "SiC Thin-Film Fabry-Perot Interferometer for Fiber-Optic Temperature Sensor," IEEE Trans. Electron Devices, **50**(10), pp. 2159–2164.
[22] Riza, N. A., and Perez, F. A., 2008, "High Temperature Minimally Invasive Optical Sensing Modules," US Patent No. 7,327,472.
[23] Riza, N. A., Arain, A., and Perez, F., 2006, "Harsh Environments Minimally Invasive Optical Sensor Using Free-Space Targeted Single-Crystal Silicon Carbide," IEEE Sens. J., **6**(3), pp. 672–685.
[24] Riza, N. A., Ghauri, F., and Perez, F., 2007, "Wireless Pressure Sensor Using Laser Targeting of Silicon Carbide," Opt. Eng., **46**(1), p. 014401.
[25] Riza, N. A., Ghauri, F., and Perez, F., 2007, "Silicon Carbide-Based Remote Wireless Optical Pressure Sensor," IEEE Photonics Technol. Lett., **19**(7), pp. 504–506.
[26] Riza, N. A., and Sheikh, M., 2008, "Silicon-Carbide-Based Extreme Environment Temperature Sensor Using Wavelength-Tuned Signal Processing," Opt. Lett., **33**(10), pp. 1129–1131.
[27] Sheikh, M., and Riza, N. A., 2008, "Experimental Studies of an All-Silicon Carbide Hybrid Wireless-Wired Optics Temperature Sensor for Extreme Environments in Turbines," *Proceedings of the Optical Sensors 2008*, Strasbourg, France, Vol. 7003, p. 70030C.
[28] Sheikh, M., and Riza, N. A., 2009, "Direct Measurement High Resolution Wide Range Extreme Temperature Optical Sensor Using an All-Silicon Carbide Probe," Opt. Lett., **34**(9), pp. 1402–1404.
[29] Riza, N. A., and Sheikh, M., 2009, "All-Silicon Carbide Hybrid Wireless-Wired Optics Temperature Sensor: Turbine Tests and Distributed Fiber Sensor Network Design," *Proceedings of the Optical Sensors 2009*, Prague, Czech Republic, Vol. 7356, pp. 73560O.
[30] Van Buren, M., and Riza, N. A., 2003, "Foundations for Low-Loss Fiber Gradient-Index Lens Pair Coupling with the Self-Imaging Mechanism," Appl. Opt., **42**(3), pp. 550–565.
[31] Lewis, R. W., Nithiarasu, P., and Seetharamu, K. N., 2004, *Fundamentals of the Finite Element Method for Heat and Fluid Flow*, Wiley, New York, p. 151.